Applied Catalysis B: Environmental 148–149 (2014) 164–169

Contents lists available at ScienceDirect

Applied Catalysis B: Environmental

journal homepage: www.elsevier.com/locate/apcatb

Elimination of BPA endocrine disruptor by magnetic $BiOBr@SiO_2@Fe_3O_4$ photocatalyst

Ling Zhang, Wenzhong Wang*, Songmei Sun, Yuanyuan Sun, Erping Gao, Zhijie Zhang

State Key Laboratory of High Performance Ceramics and Superfine Microstructures, Shanghai Institute of Ceramics, Chinese Academy of Sciences, 1295 Dingxi Road, Shanghai 200050, PR China

ARTICLE INFO

Article history:
Received 16 July 2013
Received in revised form 15 October 2013
Accepted 27 October 2013
Available online 5 November 2013

Keywords:
Bismuth oxybromine
Visible light photocatalyst
Magnetic
Bisphenol A elimination

ABSTRACT

Seeking an ideal water treatment method for endocrine disrupting compounds, which would mineralize the pollutants with least byproducts, is urgent for environmental remediation and human health. Herein, the photocatalytic elimination of 2,2-bis(4-hydroxyphenyl) propane (BPA) by $BiOBr@SiO_2@Fe_3O_4$ under the irradiation of different light sources was investigated. The experimental results revealed that the photocatalytic activity of the recyclable magnetic $BiOBr@SiO_2@Fe_3O_4$ microspheres was superior to that of commercial TiO_2 (P25) under the visible light irradiation. More importantly, only one main intermediate was detected during the photocatalytic degradation. To analyze the photocatalytic degradation mechanism of BPA, particular attention was paid to the identification of active species and intermediates. On the basis of the evidence of active species formation, a detailed degradation pathway of BPA degradation by $BiOBr@SiO_2@Fe_3O_4$ microspheres photocatalysts is proposed. This study provides a reasonable insight into the correlation between the active species and intermediated during the photocatalytic degradation process.

1. Introduction

Bisphenol A (2,2-bis(4-hydroxyphenyl) propane, abbreviated as BPA), an endocrine disruptor, is found in everything from some beverage and baby bottles to the linings of food cans [1]. Now, it has been universally found in water resources including rivers, lakes and ocean. More and more researchers reported the effects of human exposure to very low levels of BPA including reduced fertility and an increase in the incidence of breast, ovarian, and testicular cancer. Elimination of BPA from water becomes an urgent issue from the viewpoint of environmental remediation and human health even if its concentration is low [2,3]. Various methods have been suggested to remove BPA from water, such as biological method, chemical oxidation, electrochemical oxidation, and photocatalytic method [4–9]. However, it has been evidenced that if BPA was not completely mineralized, the byproducts which possess higher endocrine disrupting action would be produced during the treatment process [10]. Thus, the complete transformation of the BPA into CO_2 and H_2O is the best way for removing this pollutant.

Photocatalytic oxidation is an environmental-friendly technique in pollution control. It has been considered as an efficient tool for degrading a large number of persistent organic compounds, during which the compounds can be transformed into H_2O and CO_2 under mild conditions. On the other hand, magnetically separable photocatalyst has attracted increasing attention because of their scientific and technological importance in the environmental purification, especially in waste water treatment [11,12]. Magnetic photocatalyst could be effectively recycled by applying an external magnetic field, which avoided the secondary pollution of residue of photocatalyst in water. For example, the magnetic $TiO_2/SiO_2/Fe_3O_4$ nanoparticles which were demonstrated to be easily separable by an external magnetic field has shown photocatalytic activity to degrade acetaminophen and other four personal care products from the aqueous solution [13]. As a result, the fabrication of magnetic photocatalyst with high photocatalytic activity will be a good solution for the elimination of BPA in water.

As an efficient visible light driven photocatalyst, BiOBr receives remarkable attentions in recent years, owing to its stability, suitable band gaps and superior photocatalytic abilities in the environmental purification of organic pollutants. For example, BiOBr flakes showed unique photocatalytic abilities on the degradation of microcystin–LR (MC–LR) in water under visible light [14]. The relative research results demonstrate the potential of BiOBr in treating organic pollutant [15].

A few reports have been documented on the degradation of BPA by photocatalysis recently [16–18]. To the best of our knowledge, the report about the degradation of BPA by BiOBr still very sparse [19]. In the present study, BiOBr is considered as a component to construct a magnetic photocatalyst to eliminate BPA from

* Corresponding author. Tel.: +86 21 5241 5295; fax: +86 21 5241 3122.
E-mail address: wzwang@mail.sic.ac.cn (W. Wang).

0926-3373/$ – see front matter © 2013 Elsevier B.V. All rights reserved.
http://dx.doi.org/10.1016/j.apcatb.2013.10.053

water. Hierarchical BiOBr@SiO_2@Fe_3O_4 (abbreviated as BSF) microspheres with high photocatalytic performance were prepared by controlling synthesis conditions, and the removal efficiency, reaction kinetics, principal reaction products and degradation pathway of BPA in neutral aqueous solutions under visible light irradiation were also investigated.

2. Experimental

2.1. Materials and reagents

BPA (purity 99.5%), was purchased from Sigma Aldrich. Stock solution of BPA was prepared by dissolving a certain amount of BPA in purified water. Other materials and the chemical reagents were purchased from Shanghai reagent Co., Ltd. (China). All the chemicals were used as received without further purification. The chemicals used for the mobile phase of HPLC–MS detection included HPLC-grade methanol and acetonitrile from Dikma Chemical (China) and Mill-Q ultrapure water.

2.2. Synthesis of BiOBr@SiO_2@Fe_3O_4 microspheres

2.2.1. Fe_3O_4 microspheres

The synthesis was carried out according to a previous report with a little modification [20]. In a typical procedure, 1.35 g of $FeCl_3{\cdot}6H_2O$ was dissolved in 40 mL of ethylene glycol to form a clear solution, then 1.0 g of polyethylene glycol 20,000 and 3.6 g of $NaAc{\cdot}3H_2O$ were added. The mixture was stirred until the reactants were fully dissolved. After that, the mixture was transferred into a Teflon-lined autoclave with a capacity of 50 mL and heated at 200 °C for 8 h. The products were collected and rinsed with deionized water and ethanol for several times each, then dried under vacuum at 80 °C for 6 h.

2.2.2. Magnetic SiO_2@Fe_3O_4 composite microspheres (SF)

The synthesis was carried out according to the noted Stöber method with a little modification. Typically, 0.15 g of prepared Fe_3O_4 microspheres was dispersed in a mixture of 25 mL of ethanol and 5 mL of deionized water by ultrasonication for about 5 min. Then under continuous mechanical stirring, 1 mL of ammonia solution (25%) and 0.8 mL of tetraethyl orthosilicate (TEOS) were consecutively added to the mixture. The reaction was allowed to proceed at room temperature for 3 h under continuous mechanical stirring. The resulting products were filtered and washed, and then dried under vacuum at 80 °C for 3 h.

2.2.3. BiOBr@SiO_2@Fe_3O_4 microspheres

BiOBr layer was prepared by a simple precipitation method with $Bi(NO_3)_3{\cdot}5H_2O$ and cetyltrimethylammonium bromide (CTAB) as Bi and Br source, respectively. Briefly, 0.73 g of CTAB, was dissolved in a mixed solution of 2-methoxyethanol (96 mL), H_2O (4 mL) and SiO_2@Fe_3O_4 microspheres 0.5 g. A quantity of 0.97 g $Bi(NO_3)_3{\cdot}5H_2O$ was added to 10 mL of ethylene glycol (EG) under stirring at room temperature. After $Bi(NO_3)_3$ was dissolved completely, it was added to the mixed solution. All the reactants were sealed in a flask and maintained at 120 °C for 5 h. After cooling down to room temperature, the resulting precipitate was washed with distilled water and ethanol for several times, and dried at 60 °C for 6 h.

2.3. Characterization

The samples were characterized by X-ray powder diffraction (XRD) on a powder diffractometer (Rigaku MiniFlexII). Each sample was scanned using Cu $K\alpha$ radiation with an operating voltage of 30 kV and an operating current of 100 mA. The scan rate of 4°/min was applied to record the patterns in the range of 10°–80° at a step size of 0.01°. UV–Vis diffuse reflectance spectra were recorded on an UV–Vis spectrophotometer (Hitachi U-3010) equipped with an integrating sphere. Scanning electron microscope (SEM) characterizations were performed on a JEOL JSM-6700Felectron probe microanalyzer. Transmission electron microscope (TEM) analyses were performed by a JEOL JEM-2100F field emission electron microscope.

The photocatalytic degradation experiments were carried out in a photochemical reactor. In a typical experiment, 0.1 g of the photocatalyst was dispersed in 100 mL of BPA (20 mg/L) solution. A 500 W Xe lamp were employed as light source. For visible light experiments a 420 nm cutoff filter was used. At given time intervals, 5 mL of solution was collected from the suspension and immediately centrifuged. The concentration of BPA during photocatalytic reaction was determined by measuring the absorption of BPA solution at 276 nm using an UV–Vis spectrophotometer.

The tri-iodide production was also spectrophotochemically monitored by measuring the absorbance at 354 nm.

Triethanolamine (TEOA) is an effective hole scavenger, and isopropanol (IPA) was chosen as ·OH scavenger. Typically, 0.1 g catalyst with TEOA or IPA (10 mM) was dispersed in BPA aqueous solution (100 mL, 20 mg L^{-1}) before visible light irradiation. The concentration of BPA during photocatalytic reaction was determined by measuring the absorption of BPA solution at 276 nm. The nitroblue tetrazolium (NBT), exhibiting an absorption maximum at 259 nm, was used to determine the amount of $\cdot O^{2-}$ generating from BiOBr photocatalytic system. Photocatalytic reactions were carried out in beakers containing 1 g L^{-1} BiOBr aqueous suspensions and 5×10^{-5} mol L^{-1} NBT solution. Before the reactions, the suspensions were stirred for 1 h in dark. The production of $\cdot O^{2-}$ in BiOBr suspensions was quantitatively analyzed by detecting the concentration of NBT in the BiOBr suspensions with UV–Vis spectrophotometer.

The formation of the hydroxyl radical on the surface of the BiOBr photocatalysts under visible light irradiation was monitored by the photoluminescence (PL) technique with terephthalic acid (TA) as a probe molecule, which can readily react with ·OH to produce highly fluorescent product, 2-hydroxyterephthalic acid. The experimental procedure was similar with the photocatalytic process, except that the BPA solution was replaced by the 5×10^{-4} M terephthalic acid solution in 2×10^{-3} M NaOH. The fluorescence spectra of the formed 2-hydroxyterephthalic acid were measured by a spectrophotometer (Hitachi F-4500) excited at 315 nm.

Total organic carbon (TOC) was measured with an Elementar liquiTOC analyzer.

The HPLC–ESI–MS methods for analyzing the intermediates was performed using an Agilent 1100 MSD series equipped with an Agilent Zorbax Eclipse XDB-C18 column (2.1 mm × 100 mm, 3.5 μm).

3. Results and discussion

3.1. Characterization of the Prepared Photocatalyst

Fig. 1 shows the XRD patterns of the prepared BSF photocatalyst. All diffraction peaks in Fig. 1a are identical to the structure of the tetragonal phase BiOBr (JCPDS card No. 09–0393). In addition, the intense peaks indicate the samples are well crystallized. The diffraction peaks of Fe_3O_4 core are not detected in the composite because of the thick shell of BiOBr (0.5–2 μm, shown in Fig. S1 of Appendices A and B). In addition, the calculated weight% of Fe_3O_4 in the BSF sample was only ~7%, which is hard to be determined by the XRD instrument. SEM images of the microspheres are shown in Fig. 1b. These images of BSF spheres show that the spherical photocatalysts are different in sizes, with the diameters ranging from 2 to

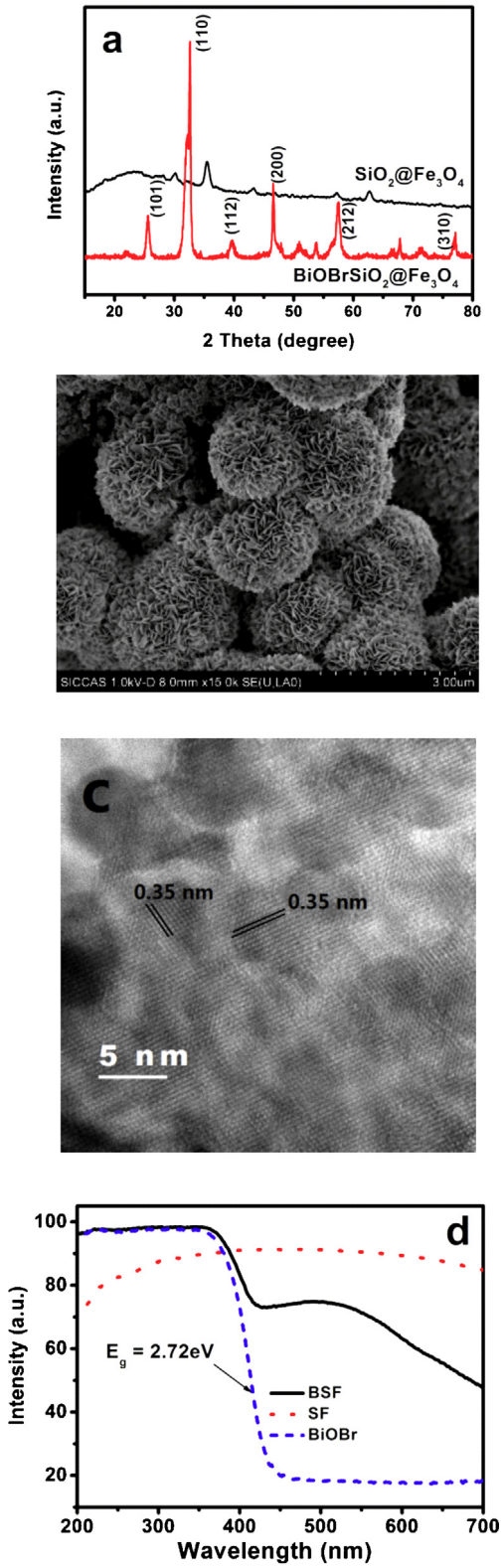

Fig. 1. (a) XRD patterns of BiOBr@SiO_2@Fe_3O_4; (b) SEM image, (c) TEM image and (d) DRS spectral of BiOBr@SiO_2@Fe_3O_4, BiOBr@Fe_3O_4 and BiOBr.

5 μm. The outer part of the microsphere is constructed by numerous thin flakes with a thickness of about 10 nm, which aggregated together to form the hierarchical assembly. High magnified TEM image (Fig. 1c) of BiOBr shows clear lattice fringes, indicating its high crystallinity, which is a characteristic of photocatalysts with high activities. The clear lattice fringes of the interplane were about 0.35 nm in the HRTEM images of BiOBr, which were in accordance with {1 0 1} planes of the tetragonal system of BiOBr. In order to avoid the recombination of photogenerated carries from the BiOBr in the Fe_3O_4 core [21,22], an "insulation" layer of SiO_2 was added between the BiOBr photocatalyst and the magnetic Fe_3O_4 core. The UV–Vis diffuse reflectance spectra of the samples were shown in Fig. 1d. The absorption spectra of the BiOBr@SiO_2@Fe_3O_4 and BiOBr@Fe_3O_4 are different due to the introduction of the SiO_2 layer. The growth of BiOBr nanoplates on the SiO_2@Fe_3O_4 microspheres slightly changed the absorption edge. The results further verify the formation of the BSF hierarchical structure. The observed absorption edge at 440 nm belongs to BiOBr, and the peaks at around 500–600 nm could be resulted from the d–d transitions of Fe in the SiO_2@Fe_3O_4 core. The band gap (E_g) of the pure BiOBr sample was estimated to be 2.72 eV from the onsets of the absorption edges using the formula:

$$\alpha h\nu = A(h\nu - E_g)^{n/2} \quad (1)$$

where α, h, ν, E_g and A are absorption coefficient, Planck constant, light frequency, band gap and a constant, respectively. Among them, n depends on the characteristics of the transition of the semiconductor. For BiOBr, the value of n is 4 for the indirect transition [23].

3.2. Photodegradation of BPA in aqueous solution

The photocatalytic activities of BSF on the degradation of BPA were investigated under visible light and UV–Vis light irradiation. Negligible degradation was detected under the UV–Vis light irradiation in the absence of the photocatalysts. It is clearly seen that after 60 min adsorption of BPA on the BSF in the dark, the concentration of BPA hardly decreased. For comparison, similar experiments were performed on P25 (TiO_2) photocatalyst. The results shown in Fig. 2a revealed that the removal rate of BPA by the BSF is close to that of the P25 under the UV–Vis light irradiation for 50 min. However, the percentage of degraded BPA is 87.0% and 27.2% by the BSF and P25 after 50 min under visible light irradiation, respectively.

Thus, BSF microspheres were superior to that of the commercial TiO_2 (P25) in the degradation of BPA under visible light irradiation.

The possibility of reuse of the photocatalysts was explored. For the recovery of the photocatalysts, BiOBr@SiO_2@Fe_3O_4 can be easily separated from the solution by a magnet (see the inset of Fig. 2b). Experimental results demonstrated that the recycled photocatalysts achieved successful removal of BPA as shown in Fig. 2b.

3.3. Active Species Involved in the Photocatalysis

In order to investigate the photocatalytic degradation mechanism of BPA by BSF, it is necessary to verify the active species involved in the photocatalysis. Here, I^- is chosen as a scavenger for valence band hole to indicate the existence of photogenerated hole. The potential of a semiconductor to photo-oxidize iodide to tri-iodide is directly related to its band gap value. In order to oxidize the iodide the hole should first react with the adsorbed iodide ion to form an iodine atom that can further react with the iodide ion to produce I_3^- [24]. Fig. 3a presents a set of experiments where the iodide was oxidized to tri-iodide by the holes under visible light irradiation. When I^- was added in the reaction solution, the photodegradation efficiency of BPA was reduced from 93.2% to 82.2% (as shown in Fig. 3b) and the concentration of the produced I_3^- decreased (as shown in Fig. 3a). This supports that photogenerated holes are one of main active species in the reaction system with BSF as photocatalyst.

However, I^- can be converted to I_3^- by not only VB hole but also ·OH radical. The experiments were carried out with TA as

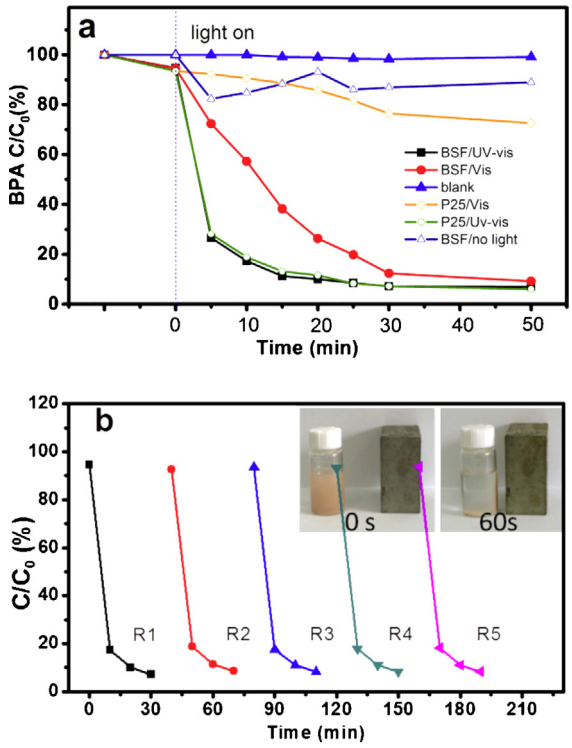

Fig. 2. (a) Photocatalytic degradation of BPA in comparison to control experiments and photocatalytic condition: (-▲-) indicates simulate solar light only; (-■-) and (-●-) indicates BiOBr@SiO_2@Fe_3O_4 under simulate solar light and visible light irradiation;(-◊-) and (-○-) indicates P25 under simulate solar light and visible light irradiation; (-△-) indicates BSF without light irradiation. (BPA: 20 mg L^{-1}; catalyst dosage, 0.1 g L^{-1}; pH7.0); (b) Recycle experiments of degrading BPA on the BSF under simulate solar light. Inset: a photograph showing magnetic recycle of the BSF photocatalyst.

a fluorescent probe to detect the presence of ·OH radical in the reaction system. ·OH radical is known to be trapped by TA to produce fluorescent 2-hydroxyterephthalic acid [25]. For comparison, the TiO_2 (P25) system was also monitored under the same conditions. Fig. 3c shows that the fluorescence intensity at ca. 425 nm is observed after 15 min illumination in the both solution. The spectrum from the BSF solution is weaker than that of TiO_2 but it has the identical shape and maximum wavelengths with that of 2-hydroxyterephthalic acid indicating the ·OH radical was indeed formed.

To investigate the photocatalysis mechanism of BPA degradation in detail, we designed and carried out different radicals and holes trapping experiments for BSF. First, triethanolamine (TEOA) was used to trap holes photogenerated in the BiOBr. As shown in Fig. 3c, at first 10 min, the degradation efficiency of BPA on BiOBr decreased significantly from 42% to 22% when TEOA was added into the photocatalytic reaction solution (curve 4), but the absorption at 276 nm increased with the increase of the reaction time. This result confirms the photogenerated holes are mainly responsible for BPA photodegradation on BiOBr. Without the direct hole oxidation, the BPA could transfer to other forms of multihydroxylated derivatives, which will result in the absorption increased in the range of 250–300 nm. Differently, the photodegradation efficiency of BPA was just reduced from 93.2% to 86.2% with the addition of ·OH scavenger IPA (curve 2), revealing that ·OH radicals play a minor role on the degradation of BPA in comparison with photogenerated holes. It is well-known that the photogenerated electrons are another key factor in photocatalytic process because they could produce superoxide and hydroxyl radicals via Eqs. (2)–(4).

$$O_2 + e \rightarrow \cdot O_2^- \quad (2)$$

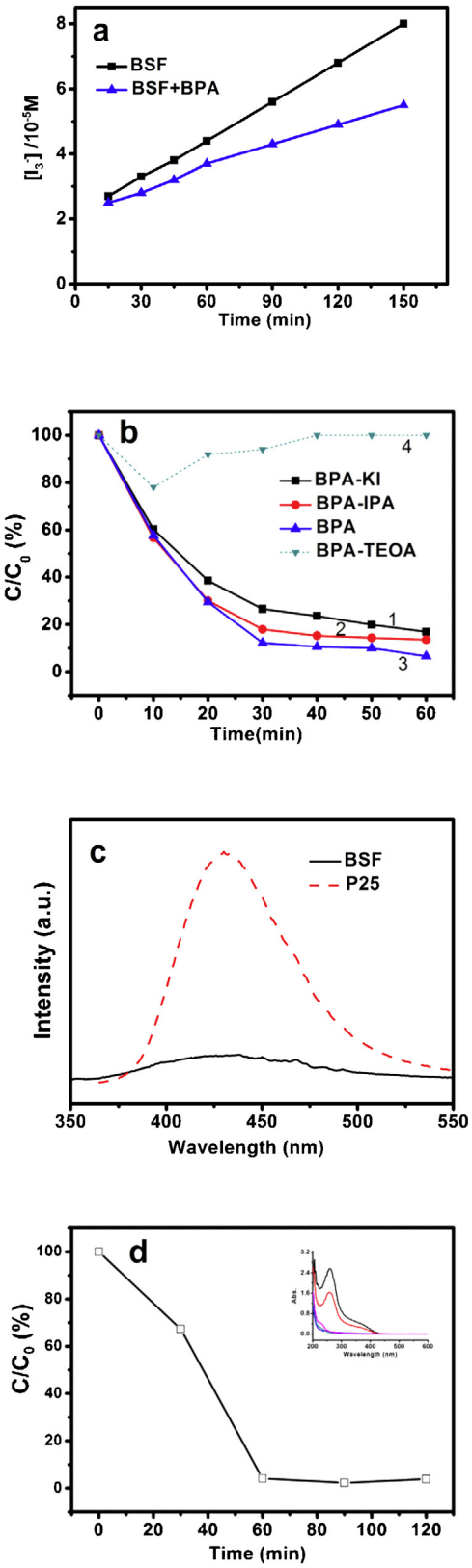

Fig. 3. (a) Photooxidation of KI (25 mmol L^{-1}) over BiOBr@SiO_2@Fe_3O_4 (-■-), and BiOBr@SiO_2@Fe_3O_4 with BPA (20 mg L^{-1}) (-▲-) under visible light irradiation; (b) Photodegradation efficiencies of BPA on BiOBr@SiO_2@Fe_3O_4 in the presence of different scavengers under visible light irradiation; (c) Fluorescence spectral of terephthalic acid in NaOH solution with BiOBr@SiO_2@Fe_3O_4 under visible light, and P25 under simulate solar light irradiation for 15 min; (d) Photodegradation of nitroblue tetrazolium (NBT) under simulate solar light (inset: UV–Vis absorption spectra of NBT during photodegradation).

$$\cdot O_2^- + e + 2H^+ \rightarrow H_2O_2 \quad (3)$$

$$H_2O_2 + e \rightarrow \cdot OH + OH^- \quad (4)$$

$$h^+ + OH^- \rightarrow \cdot OH \quad (5)$$

We therefore used the degradation of nitroblue tetrazolium (NBT) to determine the amount of $\cdot O^{2-}$ generating from BiOBr suspensions (Fig. 3d). After 2 h, about 93.3% of NBT was degraded over BiOBr under simulate solar light irradiation, confirming the generation of photoelectrons and $\cdot O^{2-}$ in under simulate solar light irradiation. Therefore, we think that ·OH radicals generated in BiOBr suspensions under simulate solar light are not from photogenerated holes, but from photogenerated electrons. It is known that the power for photogenerated electrons to generate ·OH radicals is much weaker than that of photogenerated holes, resulting in small amount of ·OH radicals produced in the BiOBr suspensions under visible light. This is why the photodegradation efficiency of BPA just slightly decreased in the presence of ·OH scavenger IPA. Therefore, we propose that direct hole oxidation and the oxidation of ·OH radicals produced via $\cdot O_2^-$ route (Eqs. (2)–(4)) are the major and minor ways for the photocatalytic degradation of BPA on BiOBr, respectively.

3.4. Photocatalytic degradation mechanism of BPA by $BiOBr@SiO_2@Fe_3O_4$

Complete mineralization of organic compounds is a great advantage of the photocatalytic treatment of organic pollutants in water. However, there are some intermediate products formed in the photocatalytic degradation process. In order to assess the photocatalytic performance of BSF to completely destruct organic molecules in water, total organic carbon (TOC) was monitored during the reaction process. As shown in Fig. 4, 83.0% of TOC was removed from the reaction system (the initial concentration of BPA was 20 ppm, pH = 7.0) after 50 min reaction with BSF under visible light irradiation while 98.0% was removed in 120 min. Photocatalytic degradation of BPA by BSF displayed an outstanding advantage in mineralization organics to CO_2 and H_2O in neutral solution.

The intermediates formed in the photocatalytic degradation process were monitored using LC–ESI–MS analysis. Except for the peak of BPA at *m*/*z* 228, only one byproduct at *m*/*z* 259 was observed during the degradation process (the detail data is shown in Appendices A and B Fig. S4). The species at *m*/*z* 259 was speculated to be multihydroxylated derivatives, which was indentified as 4-(2-(2,4-dihydroxyphenyl) propan-2-yl)benzene-1,3-diol in previous studies [16,26]. This suggests that other intermediates were

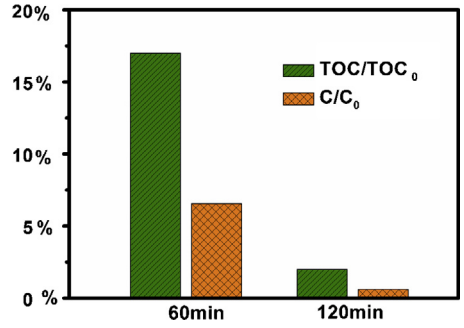

Fig. 4. Temporal concentration change of BPA and TOC removal in the presence of BSF. The initial BPA concentration was 20 ppm, the catalyst amount was 1.0 g L^{-1} in the neutral solution.

not formed or their concentrations were very low during the photocatalytic degradation by BSF photocatalyst under visible light irradiation.

The photocatalytic degradation of BPA was investigated in many previous studies. According to the literature [26,27], the hydroxyl radicals are responsible for major degradation of BPA by TiO_2 photocatalysis. The TOC conversion was limited, with less than 50% pollutant mineralization in 5 h when $TiO_2/SiO_2/Fe_3O_4$ was used as photocatalyst [13]. Guo et al. and Ohko et al. detected more than five main intermediates in the degradation of BPA by TiO_2 [17,28].Therefore more severe oxidation conditions (i.e., higher reaction time, UV lamp intensity and/or photocatalyst dose) would be needed to reach complete mineralization. Different from the degradation mechanisms of BPA by TiO_2, we propose that the degradation of BPA by BSF could be mainly due to the direct oxidation by the photogenerated holes and partly due to the hydroxyl radical oxidation. According to the results given in Section 3.3 (and k_{app} (pseudo-first-order) shown in Table S1), a possible mechanism of BPA photocatalytic degradation by BSF has been shown in Scheme 1. It can be seen that VB edge potential of BiOBr is more positive suggesting that the photo-generated hole has high oxidative potential. The degradation of BPA by holes of BSF would experience the most direct and fast pathway. First of all, BiOBr photocatalyst was irradiated and generated e^- and h^+. These e^- and h^+ pairs reacted with BPA adsorbed on the photocatalyst surface. Photogenerated holes could oxidize BPA directly to form simple organic acids, which were fast further transferred to CO_2 and H_2O. On the other hand, the formed electrons react with the adsorbed O_2 to generate $\cdot O_2^-$ and subsequently H_2O_2 [26]. There is the formation of ·OH radicals when H_2O_2 picks up an electron and a hole reacts with ·OH. The produced immediate at *m*/*z* 259, 4-(2-(2,4-dihydroxyphenyl) propan-2-yl) benzene-1,3-diol, was formed by the ·OH radicals

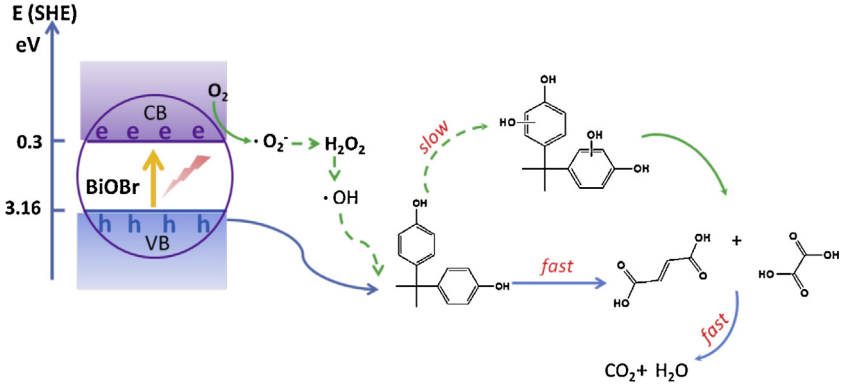

Scheme 1. Suggested degradation pathway of BPA by $BiOBr@SiO_2@Fe_3O_4$.

attacking the BPA. However, the produced ·OH is limited in this reaction system. So, this degradation path would be slower than that initiated by h^+. All in all, both the photogenerated h^+ and e^- took part in the photocatalytic degradation reaction. The degradation of BPA by BSF experienced the most direct and simple pathway comparing with the other reports [15–18], because both the photogenerated carries in the BiOBr played roles in the degradation process.

4. Conclusion

Magnetic $BiOBr@SiO_2@Fe_3O_4$ microspheres were prepared via a multi-step process. Through an analysis of the active species and intermediates in the photocatalytic degradation of BPA, a detailed and particular degradation mechanism of BPA degradation by $BiOBr@SiO_2@Fe_3O_4$ microspheres photocatalysts is proposed, which is probably unlike any previously known photocatalytic process for BPA decomposition. Only one main intermediate was detected during the photocatalytic degradation process induced by the $BiOBr@SiO_2@Fe_3O_4$ photocatalyst. It could be totally converted into CO_2 and H_2O. Thus, the "second pollution" problem of by-product was prevented in this photocatalysis. Both h^+ and ·OH were proved to be active species in the photo-reaction with BPA. The special photocatalytic reaction mechanism, that is, the direct oxidation by the photogenerated h^+ and partly due to ·OH oxidation, is proposed to be the reason for the complete and fast removal of BPA. Considering the solar energy utilization and the recycle of magnetic photocatalyst, the $BiOBr@SiO_2@Fe_3O_4$ magnetic microspheres appears to be an exciting visible light respond photocatalyst for water decontamination. The study about the relationship between the active species and intermediates during the photocatalytic process would provide a reasonable way for total mineralization of organic pollutant.

Acknowledgments

This work was supported by the National Natural Science Foundation of China (51272269, 51272303) and 973 Program (2013CB933203, 2010CB933503).

Appendix A. Supplementary data

Supplementary data associated with this article can be found, in the online version, at http://dx.doi.org/10.1016/j.apcatb.2013.10.053.

References

[1] J. Kaiser, Science 317 (2007) 884–885.
[2] A.F. Fleisch, R.O. Wright, A.A. Baccarelli, J. Mol. Endocrinol. 49 (2012) R61–R67.
[3] T. Geens, D. Aerts, C. Berthot, J.P. Bourguignon, L. Goeyens, P. Lecomte, G. Maghuin-Rogister, A.M. Pironnet, L. Pussemier, M.L. Scippo, J. Van Loco, A. Covaci, Food Chem. Toxicol. 50 (2012) 3725–3740.
[4] M.C.G. Antunes, S. Pinto, F.G. Braga, J. Silva, Chem. Ecol. 28 (2012) 141–152.
[5] L. Joseph, Q. Zaib, I.A. Khan, N.D. Berge, Y.G. Park, N.B. Saleh, Y. Yoon, Water Res. 45 (2011) 4056–4068.
[6] Y. Kimura, M. Yamamoto, R. Shimazaki, A. Kashiwada, K. Matsuda, K. Yamada, J. Appl. Polym. Sci. 124 (2012) 796–804.
[7] J. Lee, S. Hong, Y. Mackeyev, C. Lee, E. Chung, L.J. Wilson, J.H. Kim, P.J.J. Alvarez, Environ. Sci. Technol. 45 (2011) 10598–10604.
[8] H. Melcer, G. Klecka, Water Environ. Res. 83 (2011) 650–666.
[9] B. Seyhi, P. Drogui, G. Buelna, J.F. Blais, Sep. Sci. Technol. 87 (2012) 101–109.
[10] J.Y. Hu, T. Aizawa, S. Okubo, Environ. Sci. Technol. 36 (2002) 1980–1987.
[11] S.Q. Liu, Environ. Chem. Lett. 10 (2012) 209–216.
[12] P.A. Xu, G.M. Zeng, D.L. Huang, C.L. Feng, S. Hu, M.H. Zhao, C. Lai, Z. Wei, C. Huang, G.X. Xie, Z.F. Liu, Sci. Total Environ. 424 (2012) 1–10.
[13] P.M. Alvarez, J. Jaramillo, F. Lopez-Pinero, P.K. Plucinski, Appl. Catal., B 100 (2010) 338–345.
[14] Y.F. Fang, Y.P. Huang, J. Yang, P. Wang, G.W. Cheng, Environ. Sci. Technol. 45 (2011) 1593–1600.
[15] J. Xu, W. Meng, Y. Zhang, L. Li, C. Guo, Appl. Catal., B 107 (2011) 355–362.
[16] C.Y. Wang, H. Zhang, F. Li, L.Y. Zhu, Environ. Sci. Technol. 44 (2010) 6843–6848.
[17] C.S. Guo, M. Ge, L. Liu, G.D. Gao, Y.C. Feng, Y.Q. Wang, Environ. Sci. Technol. 44 (2010) 419–425.
[18] C. Wang, L. Zhu, M. Wei, P. Chen, G. Shan, Water Res. 46 (2012) 845–853.
[19] H.T. Tian, J.W. Li, M. Ge, Y.P. Zhao, L. Liu, Catal. Sci. Technol. 2 (2012) 2351–2355.
[20] H. Deng, X.L. Li, Q. Peng, X. Wang, J.P. Chen, Y.D. Li, Angew. Chem. Int. Ed. 44 (2005) 2782–2785.
[21] K. Laohhasurayotin, S. Pookboonmee, D. Viboonratanasri, W. Kangwansupamonkon, Mater. Res. Bull. 47 (2012) 1500–1507.
[22] Q. Yuan, N. Li, W.C. Geng, Y. Chi, X.T. Li, Mater. Res. Bull. 47 (2012) 2396–2402.
[23] L. Zhang, X.F. Cao, X.T. Chen, Z.L. Xue, J. Colloid Interface Sci. 354 (2011) 630–636.
[24] G.T. Li, K.H. Wong, X.W. Zhang, C. Hu, J.C. Yu, R.C.Y. Chan, P.K. Wong, Chemosphere 76 (2009) 1185–1191.
[25] S. Shenawi-Khalil, V. Uvarov, Y. Kritsman, E. Menes, I. Popov, Y. Sasson, Catal. Commun. 12 (2011) 1136–1141.
[26] C. Tai, G. Jiang, J. Liu, Q. Zhou, J. Liu, J. Photochem. Photobiol., A 172 (2005) 275–282.
[27] L. Yang, L.E. Yu, M.B. Ray, Environ. Sci. Technol. 43 (2009) 460–465.
[28] Y. Ohko, I. Ando, C. Niwa, T. Tatsuma, T. Yamamura, T. Nakashima, Y. Kubota, A. Fujishima, Environ. Sci. Technol. 35 (2001) 2365–2368.